Optics Communications 284 (2011) 3539–3547

Contents lists available at ScienceDirect

Optics Communications

journal homepage: www.elsevier.com/locate/optcom

On the compensation of chirp induced from semiconductor optical amplifier on RZ data using optical delay interferometer

K.E. Zoiros [a,*], Z.V. Rizou [a], M.J. Connelly [b]

[a] Lightwave Communications Research Group, Department of Electrical and Computer Engineering, School of Engineering, Democritus University of Thrace, 12 Vas. Sofias Str., 67 100, Xanthi, Greece
[b] Optical Communications Research Group, Department of Electronic and Computer Engineering, University of Limerick, Limerick, Ireland

ARTICLE INFO

Article history:
Received 14 December 2010
Received in revised form 27 March 2011
Accepted 28 March 2011
Available online 11 April 2011

Keywords:
Optoelectronic devices
Semiconductor optical amplifier
Pattern effect
Chirp
Optical delay interferometer
Modeling

ABSTRACT

The capability of an optical delay interferometer (ODI) to compensate the chirp induced on return-to-zero pulses amplified by a semiconductor optical amplifier (SOA) when operated under stressful conditions for its gain dynamics is investigated and demonstrated through extensive numerical simulation. The phase response of the ODI, which through its variation per time increment determines the chirp, is calculated at its crossed output port using an explicit expression. The theoretical analysis reveals that cascading the ODI after the SOA can reduce both the magnitude of the chirp and the variations of its peaks as well as those of the amplified pulses while ensuring error-free performance even for a tight combination of the critical parameters. In order for this goal to be successfully accomplished while not distorting the pulses acted on by the ODI the offset introduced by this passive element is computationally found that it must not exceed 10% of their repetition interval. Therefore the scheme can constitute a promising technological option for efficiently exploiting the chirp of an SOA and simultaneously using the SOA as gain block for direct amplification purposes.

1. Introduction

In last years the significant progress realized in the field of semiconductor optical amplifiers (SOAs) has made these active devices exhibit multi-functional capability, low power consumption, small footprint, wide gain bandwidth and integrability [1]. These attractive technological characteristics have spurred in turn intense research efforts for their deployment as power boosters [2,3], in-line amplifiers [4–6] and preamplifiers [7,8], with the ultimate goal to assist the implementation of lightwave communication systems and networks. However, their efficiency in these applications is constrained by the pattern effect that occurs due to the strong saturation and incomplete recovery of their gain in between excitation pulses of random binary content [9]. Among the various methods we have recently proposed [10–12] to resolve this problem and enable the unobstructed exploitation of a stand-alone conventional SOA in its classical role, the use of an optical delay interferometer (ODI) with its appealing features [13] is a very promising option. This potential has been demonstrated both theoretically [13] and experimentally [12] for the case of return-to-zero (RZ) data format. The ODI is serially placed after the SOA acting as a filter to properly suppress the spectral components of the unevenly amplified pulses that have been broadened under heavy saturation condition due to the manifestation of self-phase modulation (SPM), thus canceling the source of pattern-dependent distortion [14,15]. In this manner the amplitude wandering at the SOA exit, quantified by the amplitude modulation (AM), can be kept below an acceptable level [10–13]. This in turn allows the input power dynamic range of the SOA to be extended beyond the quasi-linear regime, where it should otherwise be operated for its gain to be unaffected by irregular variations at the expense of low output power and optical signal-to-noise ratio degradation [16,17]. On the other hand, the nonlinear phenomenon of SPM also imposes a chirp on a pulse whose intensity is relatively high with respect to the saturation level of a SOA via which it is propagated [18]. This quantity can be useful for mitigating the deleterious consequences of chromatic dispersion, hence extending the maximum reach of a fiber link [19]. Also it can enable pulse compression when its counterpart introduced in a suitable dispersive medium has the opposite sign [20]. However when the SOA is driven by a stream of pulses having alternating logical value and not by a train of continuous pulses or by just a single pulse then this potential is compromised. The reason is that due to the abnormal change of its gain dynamics that occurs in this case the physical mechanism leading to chirp is affected in a similar fashion. Accordingly the fluctuations in the peaks of the resultant pulses are also transferred to the chirp

* Corresponding author. Tel.: +30 25410 79 975; fax: +30 25410 79 595.
E-mail address: kzoiros@ee.duth.gr (K.E. Zoiros).

0030-4018/$ – see front matter © 2011 Elsevier B.V. All rights reserved.
doi:10.1016/j.optcom.2011.03.072

whose amplitude is thus not identical from pulse to pulse. Therefore in order to be able to take advantage of this induced instantaneous frequency deviation its uniformity in the bit slots containing a mark should definitely be enhanced. In this context it would also be desirable if its magnitude were simultaneously reduced. This for example would be necessary for avoiding degrading the performance of an all-optical switch [21] when an SOA is utilized as linear gain block to provide the necessary energy to the signal that determines switching [22]. For this purpose we propose in this paper to adopt the concept based on the ODI and theoretically investigate whether and to what degree it would be capable of compensating the chirp in the way mentioned before. The idea of using an optical filter, which the ODI essentially is, directly after an SOA to properly engineer the chirp imposed on the pulses passing through, has been undertaken before. However this has been done in various applications of SOA-based switches whose operation relies on the change of the SOA response incurred by one signal and suffered by another [23–29]. On the contrary in our case the modification of the SOA gain dynamics is provoked by a data-modulated signal onto itself, and so the approach required for removing patterning is different from a physical perspective. Compared also to previous works that deal with the complications of straightforward amplification using optical filtering [14,15,30–33], their primary concern has been to show the potential of the technique to alleviate the pattern effect only on the amplified pulses and not regarding the chirp as well. Thus in this paper our effort is focused on the chirp at the crossed output port of the cascaded ODI, aiming at thoroughly investigating its impact and optimally compensating its effect through its explicit treatment. This goal is methodically achieved by means of a numerical model validated through succinct comparison with available experimental evidence [12]. Furthermore, an analytical expression similar to that in [34] is used for the ODI phase response, whose variation per time increment determines chirp. In this manner it has been possible to assess the impact of the time delay inserted by the ODI on the chirp and specify the value that is appropriate for satisfying most the requirements defined for this parameter while simultaneously ensuring a tolerable AM. The outcome of this work can be helpful for allowing SOAs to better serve the needs of direct signal amplification for which they have been traditionally destined.

2. Principle of operation

The setup considered in this work is schematically shown in Fig. 1, and consists of a data-driven SOA and a concatenated ODI. In this configuration there are three points of interest, which are denoted by A, B and C and are located at the SOA input, SOA output and just after the ODI, respectively. At each one of them a set of traces is depicted both in the time (pulse waveform and eye diagram (ED)) and frequency (spectrum, including the ODI response, and chirp) domain. The information contained in them is available, experimentally from [12] and the details therein for the three first cases, and theoretically for the last one from the simulation conducted in this paper as described in the next section.

The data signal, which is characterized by high quality in terms of the aforementioned features, i.e. low AM [13], open ED with high extinction ratio (ER), symmetric spectrum and no chirp, is launched into the SOA from point A. If its power and temporal content are such that the SOA is highly saturated, then due to the SOA finite gain recovery time the SOA output depends on the logical values of the preceding input data bits instead of solely on the current input bit. The undesirable by-product of this situation is the severe performance deterioration at point B, which is directly reflected on the non-uniform profile of the amplified pulses. These are governed by intense amplitude excursions and a poor quality ED that is deformed to secondary envelopes. Furthermore, the strong gain saturation responsible for this pattern effect causes through the process of SPM the exit pulses to be spectrally broadened to the longer wavelength side and accordingly acquire a chirp. This is negative in the leading edge (red chirp) of the pulse, almost linear with increasing slope in its central part and positive in its trailing edge (blue chirp). The red chirp is related to carrier depletion and gain compression while the blue chirp is linked to carrier regeneration and gain recovery [24]. Since in

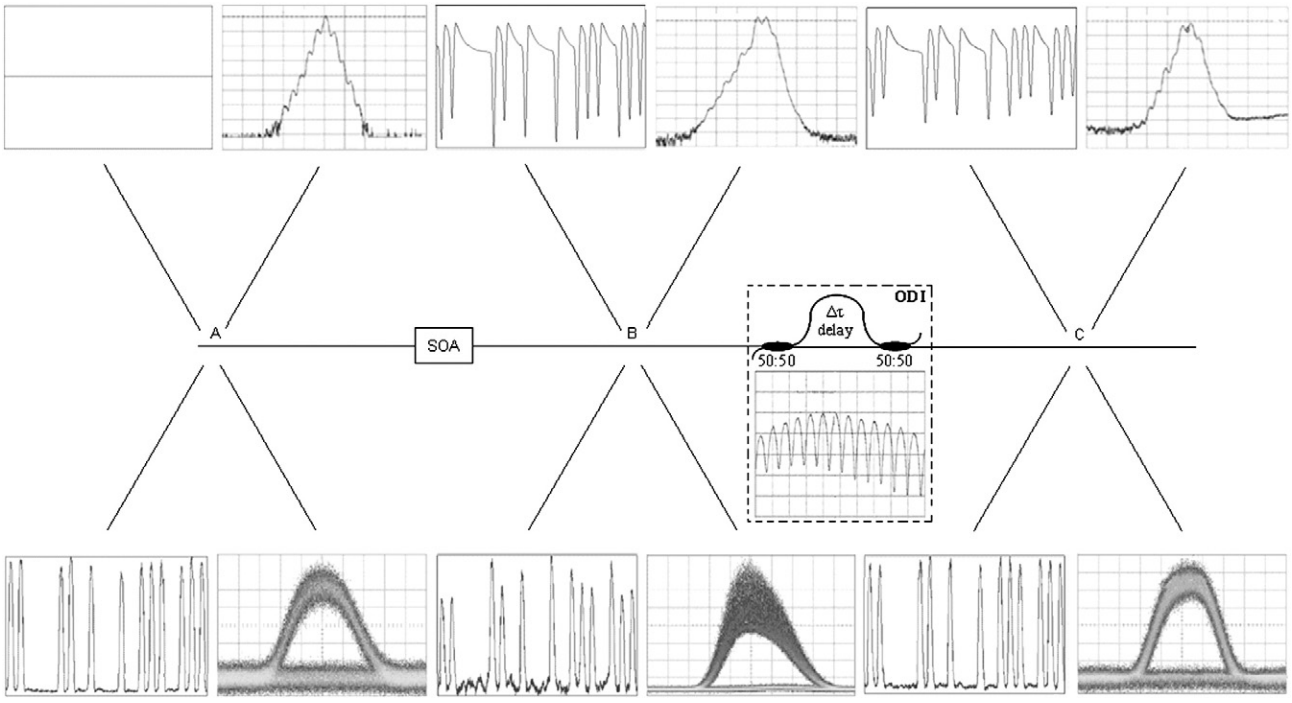

Fig. 1. Configuration of serially connected SOA and ODI considered in the simulation. The frames shown at different locations along the setup are representative for the data pulse train, the eye diagram, the spectrum and the chirp: before SOA (A), after SOA (B) and after ODI (C). The spectral response of the ODI is also shown below it.

the presence of pattern effect the change of the carrier concentration and subsequently of the gain occurs in an irregular fashion, this means that under such circumstances the amount of chirp should also be similarly affected. However, due to the different time scale on which the two types of chirp take place [26], the red chirp is substantially larger and suffers more from peak excursions than the blue one, which remains closer to the position of the input carrier frequency and has nearly the same magnitude.

The previous physical behavior designates that the root of the problem is the broadening of the spectrum and the associated unequal peaks of the red chirp. This in turn suggests that if the former could be canceled then the latter would be suppressed and the pattern effect would be combated. This can be done by filtering out the red-shifted components without impairing the central wavelength while favoring the blue ones but without being converted into amplitude information [31]. Here is where the ODI can be employed to satisfy these requirements by exploiting its frequency discrimination capability. More specifically, the ODI is constructed by connecting two 3 couplers with a length difference between the upper and lower arms that results in a relative time delay, $\Delta\tau$. When the signal coming out from the SOA is fed into the ODI, the two identical copies into which it has been split reach its rear end at different times. This creates a phase difference between them given by [35] $\Delta\varphi=(2\pi c\Delta\tau)/\lambda$, where c is the speed of light in vacuum and λ is the operating wavelength. Thus on their recombination the result is a function of the wavelength and consists of alternating maxima and minima depending on how close $\Delta\varphi$ is to an even or odd multiple of π, respectively. The spacing or free spectral range (FSR) between these points is inversely proportional to $\Delta\tau$, as expressed by [35] $FSR=\lambda^2/(c\Delta\tau)$. This form of the ODI response allows to exploit it as a notch filter to cancel the spreading of the spectral components towards the longer sideband and the associated pattern-dependent degradation. This can be done by biasing, with the appropriate choice of $\Delta\tau$, the ODI at the quadrature point with negative slope versus the optical carrier wavelength in the transmission characteristic [36] so that the frequency–amplitude conversion compensates the gain saturation. In this manner these spectral components are pushed to fall around the nulls, which are located at the middle of the FSR, thereby being attenuated in direct analogy to the degree of their shift. Therefore the ODI action suppresses the red-shifted spectral peaks repositioning the spectrum to its initial center. The closer the latter is approached the more the red chirp is reduced and its peak fluctuations become less intense. This fact is translated to a better AM of the amplified data stream, which as desired is transformed to quite an enhanced replica of the original one, while the ED is restored to resemble that before the SOA. Thus the achievement of these performance improvements at point C compared to point B clearly underscores the significant contribution of the ODI in relaxing the detrimental impact of the pattern effect, in particular concerning the chirp.

3. Model formulation

The employed model aims at simulating the chirp at the output of the SOA and of the ODI within the frame of their joined setup. For this purpose the analysis starts from the fact that this quantity is mathematically given by the time derivative of the phase modulation, F(t) [18]

$$\Delta\nu(t)=-\frac{1}{2\pi}\frac{dF(t)}{dt}. \tag{1}$$

This general equation indicates that the calculation of the instantaneous frequency deviation of the pulses emerging from each one of the involved elements requires the knowledge of their phase transfer function, which is addressed in the following.

For the case of an SOA, it is known that its phase response, $F_{SOA}(t)$, is linked to the integrated gain response, h(t), through the linewidth enhancement factor, α_H [18]

$$F_{SOA}(t)=-\frac{1}{2}\alpha_H h(t) \tag{2}$$

where h(t) is described by the first-order differential equation obtained after the necessary assumptions have been made [37]

$$\frac{dh(t)}{dt}=\frac{\ln(G_{ss})-h(t)}{T_{carrier}}-\frac{P_{data}(t)}{E_{sat}}\{\exp[h(t)]-1\} \tag{3}$$

and G_{ss}, $T_{carrier}$ and E_{sat} are the SOA unsaturated single-pass power gain, carrier lifetime and saturation energy, respectively. A closed-form solution to formula (3) can be obtained if the width of the data pulses introduced in the SOA is much smaller than its carrier lifetime [18]. However this does not happen in our case [12] where a pronounced pattern effect is provoked not only by the power of the data pulses, $P_{data}(t)$, but by their temporal content as well. More precisely, their full-width at half-maximum (FWHM), T_{FWHM}, is 27 ps and consequently the difference from their repetition interval, 100 ps at the considered data rate of 10 Gb/s is less than the SOA gain recovery time of 75 ps. This results in a more demanding operational situation for the SOA gain dynamics, which follows more slowly the alternating logical values of pulses having wider width, thus aggravating the pattern effect [23]. Since the ultimate goal of modeling is to reproduce the experimental conditions as realistically and accurately as possible, this means that the only way of solving Eq. (3) is by a numerical approach. This can be done in a step-wise manner by sampling the optical pulse over its period at discrete temporal intervals, approximating the time derivative by a finite difference and applying the appropriate initial conditions to account for the different gain at the beginning of each new bit depending on how it has been perturbed during the previous one [38]. The input signal used in this procedure is a Gaussian-shaped pseudorandom binary sequence (PRBS) of word length 2^7-1

$$P_{data}(t)=\sum_{n=1}^{2^7-1}\{C_n\}P^1_{peak}\exp\left[-\frac{\left(t-n^{T_{period}}/_2\right)^2 4\ln 2}{T^2_{FWHM}}\right] \tag{4}$$

where the digital code $\{C_n\}$ symbolizes the logical value of the n-th bit contained in the data stream, which is either '1' or '0' with equal probability. The format of the pulses is RZ so as to preserve the continuity with our previous relevant work [10–13], but also because this coding is preferable in terms of better receiver sensitivity and transmission performance compared to its NRZ on–off keying alternative [39,40], for which the nature of the pattern effect that has been addressed in [30] is less complicated [12,13]. Given now that in practice the quantity measured by the diagnostic equipment is the average power, P_{ave}, it is necessary to define its relation to the peak power of the marks, P^1_{peak}, in order to be able to make the transition between experiment and theory in a straightforward manner. For a modulated pulse train, like the one generated according to the method described in [10–12], this is [41] $P_{ave}=P^1_{peak}(1+1/\zeta)/2D$, where $\zeta=P^1_{peak}/P^0_{peak}$ is the extinction ratio between the marks and spaces and $D=T_{period}/T_{FWHM}$ is the duty factor. Thus by using Eq. (4) in Eq. (3), the values of h(t) can be arithmetically computed. Then they are replaced in Eq. (2), whose variation per time increment gives according to Eq. (1) the chirp at the output of the SOA, and in the expression for the amplified output [18]

$$P_{SOA}(t)=P_{data}(t)\exp[h(t)]. \tag{5}$$

The ODI, on the other hand, is a type of frequency discriminator whose product at its crossed output port when it receives a signal like

Eq. (5) in our case is the sum of the power contribution from each interferometric path and an interference term [13,42]

$$P_{ODI}(t) = \frac{1}{4}\left\{P_{SOA}(t) + P_{SOA}(t-\Delta\tau) + 2\sqrt{P_{SOA}(t)P_{SOA}(t-\Delta\tau)}\cos[\Delta F(t)]\right\} \quad (6)$$

where $\Delta F(t) = F_{SOA}(t) - F_{SOA}(t-\Delta\tau)$. This equation is adequate for describing the intensity of the signal at the ODI exit but it does not give us any information about its phase, which however should be known as it is required to find the corresponding chirp from its temporal change according to Eq. (1). This can be specified by following an approach analogous to that in [43] but adapted to a passive element like the ODI, which involves working with the electric fields of the principal signal and its delayed counterpart while manipulating in the proper algebraic manner the terms of the phase shift that these components experience as they traverse the ODI and recombine. The result that is obtained after some cumbersome algebraic manipulations is the phase response of the ODI at its crossed output port

$$F_{ODI}(t) = F_{SOA}(t-\Delta\tau) - \arctan\left\{\frac{1+\sqrt{P_R(t)}\cos[\Delta F(t)]}{\sqrt{P_R(t)}\sin[\Delta F(t)]}\right\} \quad (7)$$

where $P_R(t) = \dfrac{P_{SOA}(t)}{P_{SOA}(t-\Delta\tau)}$. Since the functions contained in this formula are all well defined and known the chirp that occurs at the ODI output can be analytically calculated by taking the time derivative of Eq. (7) and substituting it in Eq. (1) so that the task of modeling is finally completed.

4. Model validation

Before applying the formulated model to obtain simulation results, we verify that it is indeed appropriate to be employed with a high degree of confidence. This is done by comparing its outcome against experimental evidence available for the SOA operation in the most extreme case so as to check if there is a good agreement. The values of the SOA parameters involved in this procedure and replaced in the model are those of the 1000 μm-long commercial device used in [10–12], where the setup up to the SOA exit is the same. More specifically, these are $G_{ss} = 23$ dB, $T_{carrier} = 75$ ps, $E_{sat} = 1.5$ pJ and $\alpha_H = 8$, which are treated as fixed throughout the simulation. Similarly the specifications of the signal launched into the SOA are $T_{period} = 100$ ps, $T_{FWHM} = 27$ ps, and $P_{ave} = -2$ dBm, which combined with $\zeta = 20$ dB is equivalent to $P^1_{peak} = 4.6$ mW ($\simeq 6.6$ dBm) and hence well above the SOA 3 dB saturation input power of −7 dBm. These power and temporal characteristics together provoke a pronounced pattern effect at the SOA output since the former brings the SOA into deep saturation, while the latter corresponds to a difference between the pulse repetition period and FWHM smaller than the SOA gain recovery time.

By using as input the experimental pulse launched into the SOA, which is plotted in Fig. 2 (left) with a resolution of 3294 time points after it has been reconstructed from the data stored in a Digital Communications Analyzer (DCA), the model was run to compare the individual amplified pulse that it produces with that obtained in reality. Fig. 2 (right) shows that there is good fit between the profiles of the two pulses since their borders almost coincide, while unlike the perfect input both of them have an asymmetric envelope due to the different gain encountered and perturbed by their leading and trailing edges under strong pattern effect [18]. The model can also predict correctly the SOA output for the heavy saturation conditions defined above, as it can be verified from Fig. 3 by comparing the experimental to the theoretical amplified pulse trains as well as eye and pseudo [42]-eye diagrams, respectively, obtained in this case. Clearly there is a good qualitative matching between them, and the model additionally reproduces the exact form of the pattern effect manifested on RZ pulses [10–12].

5. Results

After the validity of the model has been confirmed, we proceed in a concise manner with the obtained results focusing on the chirp and its compensation. The primary goal is to find the proper time delay, $\Delta\tau$, so as to manipulate the red chirp in the most favorable way for the scopes of this paper. At the same time the AM of the amplified pulses must be kept below its typical maximum [13] so as to avoid the performance degradation detailed in [44], which in particular can be quite detrimental when cascading several SOAs [45,46]. To this aim a 9 bit-long data frame of 111010001 inside the PRBS has been selected for convenience of visual representation while ensuring a reasonable number of bits gathered in each diagram.

Fig. 4 shows pairs of amplified pulses and induced chirp for different values of $\Delta\tau$. For the SOA alone, i.e. $\Delta\tau = 0$ ps (a), the pattern effect on both of them is severe and therefore as they stand are unacceptable. Nevertheless the connection of the ODI after the SOA improves things since compared to its absence not only the relative intensity differences are considerably alleviated, as quantified by the reduction of the AM to 0.18 dB from ~1 dB for $\Delta\tau = 9$ ps (b), but also the variations of the red chirp are compensated and its absolute maximum magnitude is reduced. In particular the peaks of the chirp for the marks that follow directly after a mark become more balanced, the fluctuations between the chirp imposed on marks that are separated by a run of zeros become smaller and the maximum and minimum peaks across the bit stream diverge less from each other. On

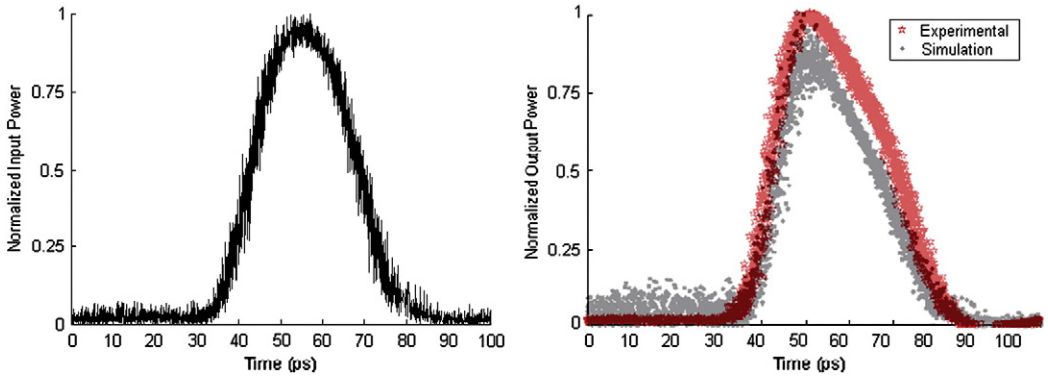

Fig. 2. Individual pulse comparison: (left) experimental pulse launched into the SOA and used as input to the model; (right) amplified pulse obtained from model (gray) and experiment (red).

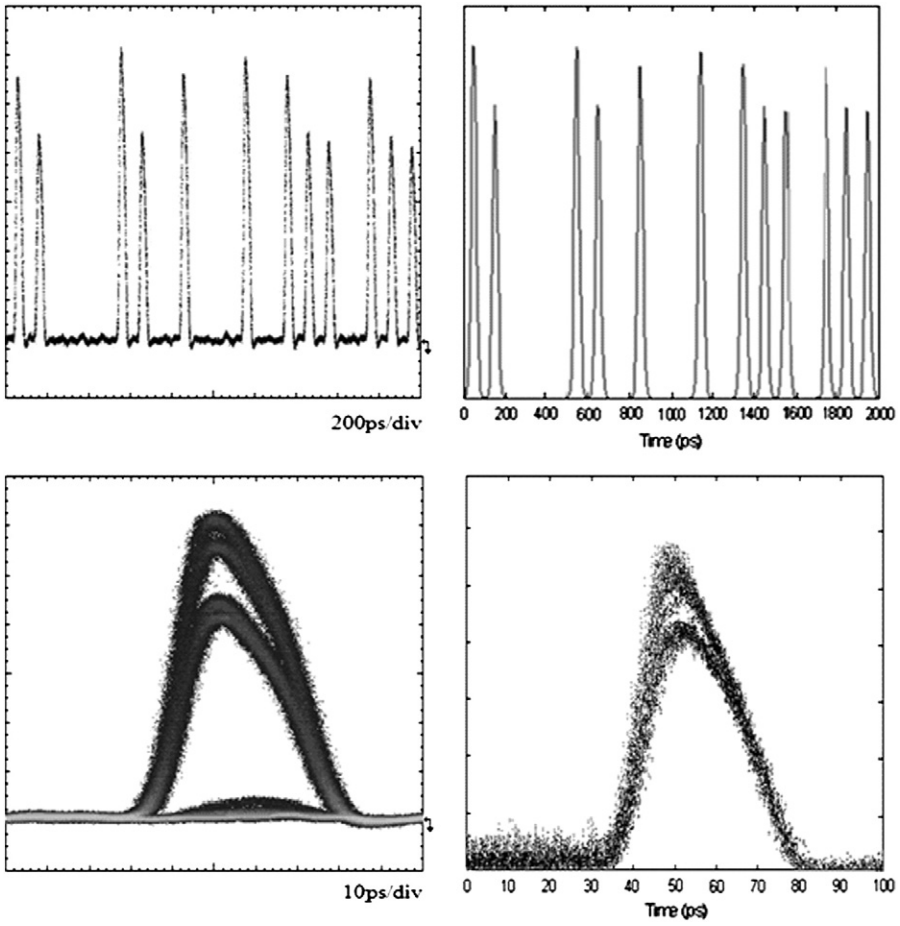

Fig. 3. Comparison between experimental and theoretical amplified data pulse trains (top) as well as eye and pseudo-eye diagrams (bottom) obtained from DCA (left column) and simulation (right column), respectively, for SOA deep saturation. The simulation results have been taken using the representative 20 bit-long segment of 11000110100101110111 in the first case, and the experimental pulse launched into the SOA according to Fig. 2 (left) in the latter.

the other hand, if $\Delta\tau$ is increased further the chirp and pulse profiles become strongly distorted, and even secondary pulses come into being within the same period, as it is noticed for $\Delta\tau = 15$ ps (c). The physical reasoning for this undesirable situation is twofold. More specifically, in the time domain, the more $\Delta\tau$ approaches the FWHM that concurrently occupies a sizeable portion of the allocated bit slot, as in our case, the more difficult is for the data signal entering the ODI to catch up and interfere properly with its delayed replica. In this manner the pattern effect suppression mechanism does not function properly, thus impairing the quality of the transmitted pulses and compromising the effectiveness of chirp compensation, which is likewise affected. Similarly in the frequency domain the filtering action of the ODI to suppress the red-shifted spectral components comes at the expense of inevitably losing some information contained in them. This happens because for larger $\Delta\tau$ these components are forced to lie in a segment of the negative slope in the ODI wavelength transfer function that is steeper, thus undergoing a greater insertion loss [36]. Therefore there is an upper limit in the amount of $\Delta\tau$, which should be close to, but not surpass, 10 ps (d) in order to satisfy the performance requirements simultaneously for the amplified pulses and the chirp imposed on them. This finding also holds for the Q-factor, which is defined as [47]

$$Q = \frac{\bar{P}_1 - \bar{P}_0}{\sigma_1 + \sigma_0} \tag{8}$$

where $\bar{P}_1$, $\bar{P}_0$ and σ_1, σ_0 are the mean and the standard deviation of the peak power of the marks and spaces, respectively, in the data train at the points of interest. The variation of this metric against the time delay inserted by the ODI has been plotted in Fig. 7 to monitor how it is affected by the specific critical parameter. From the observation of the curve it is evident that under strong pattern effect it is not possible for the Q-factor obtained at the output of the SOA alone to exceed the limit of six. This is required to ensure that the directly related bit error rate (BER) is smaller than 10^{-9} [47] and hence more than adequate for the target applications of straightforward amplification. Nevertheless, the use of the ODI can be beneficial for the Q-factor and the performance of the scheme. This can be realized by making the approximation [34]

$$\Delta F(t) = F_{SOA}(t) - F_{SOA}(t-\Delta\tau) \sim \Delta\tau \frac{dF_{SOA}(t)}{dt} \tag{9}$$

which is valid when $\Delta\tau$ is small compared to the period of the modulated data [36], as it happens in this work. Then it is possible to rewrite formula (6) for the ODI output power, which is involved in the definition of the considered metric, as

$$P_{ODI}(t) = \frac{1}{4}\left\{P_{SOA}(t) + P_{SOA}(t-\Delta\tau) + 2\sqrt{P_{SOA}(t)P_{SOA}(t-\Delta\tau)}\cos\left[\Delta\tau\frac{dF_{SOA}(t)}{dt}\right]\right\}. \tag{10}$$

Since the term $\frac{dF_{SOA}(t)}{dt}$ represents from Eq (1) the SOA chirp, it can be deduced that the previous function and hence the Q-factor depends on this parameter. Therefore the chirp changes caused by $\Delta\tau$ will affect the Q-factor and the improvement achieved for the

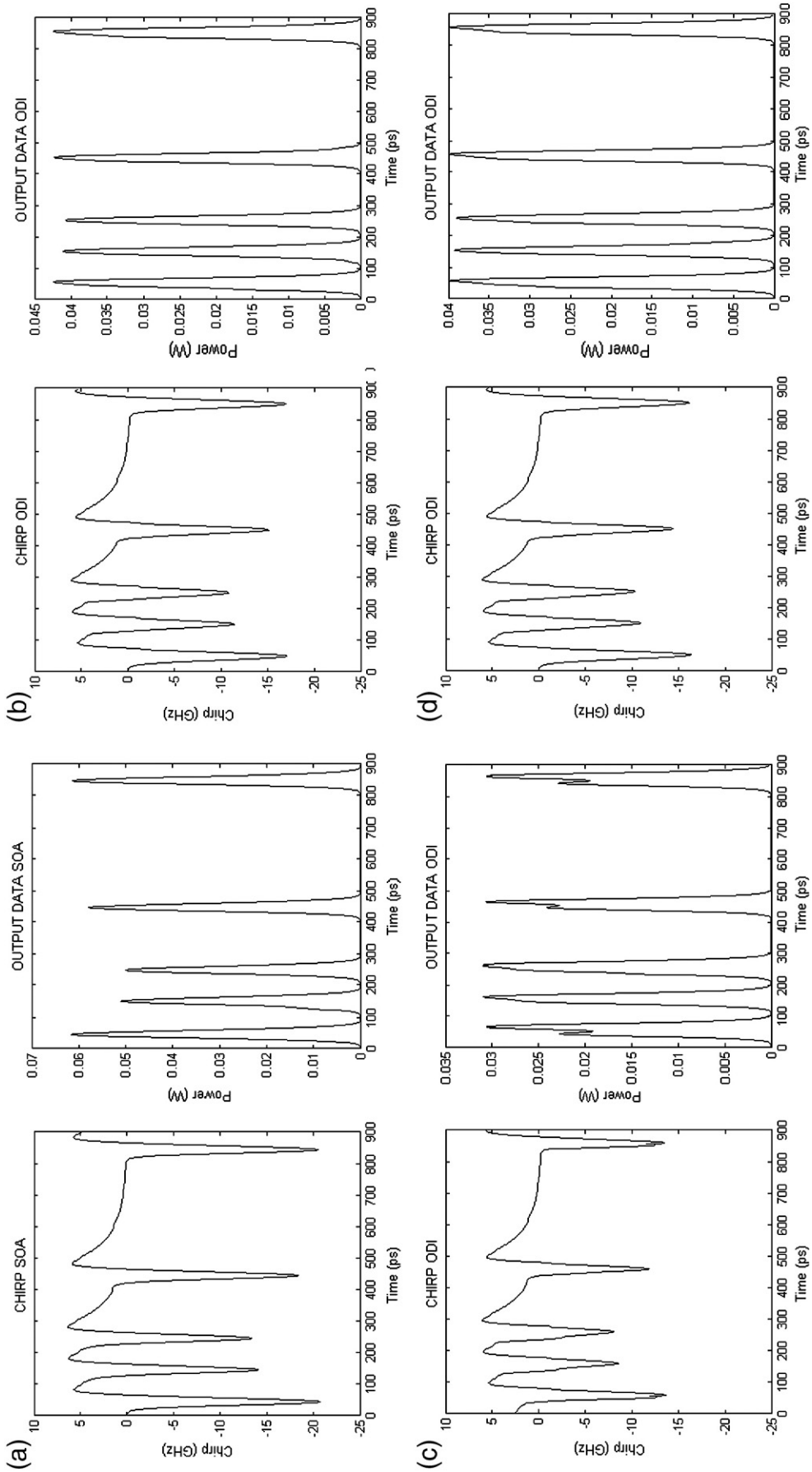

Fig. 4. Amplified output chirp (left) and pulse (right) profiles, without ODI-$\Delta\tau = 0$ ps (a), and with ODI that inserts time delay $\Delta\tau = 9$ ps (b), $\Delta\tau = 15$ ps (c) and $\Delta\tau = 10$ ps (d).

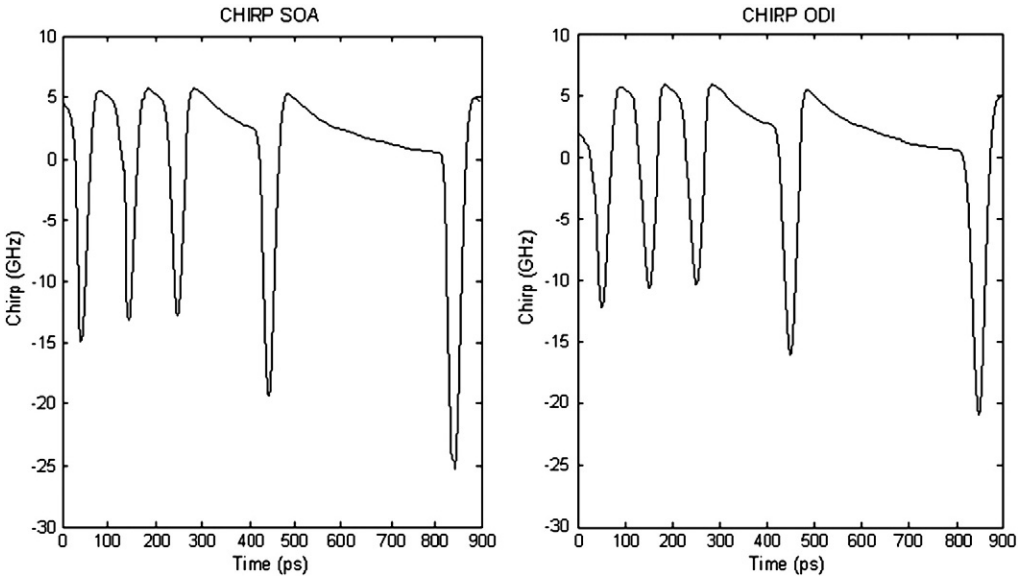

Fig. 5. Amplified output chirp profile for tight SOA working condition in terms of the selected critical parameters, without ODI ($\Delta\tau = 0$ ps) and with ODI of proper time delay ($\Delta\tau = 9$ ps).

former will be reflected on the latter. In fact, with the introduction of $\Delta\tau$, the Q-factor is progressively ameliorated and becomes acceptable at approximately 2.9 ps, where however it is not possible to achieve sufficient pattern-free operation as well. From this point onward the continuous growth of $\Delta\tau$ has a drastic influence since the Q-factor follows an inclined course in an exponential-like manner and is maximized at 9 ps, beyond which its calculation has no meaning due to the aforementioned pulse distortion. This behavior is in agreement with that governing the performance of the considered scheme with respect to the chirp and amplitude modulation, and is again ascribed to the ODI function in the time and frequency domains. Therefore all evidence confirms the impact of the ODI temporal offset as it is altered and justifies its optimum choice for performance improvement, so that we can feel strongly confident about the model's predictions.

Furthermore, we investigated the efficiency of the proposed scheme to compensate the chirp when the working condition of the SOA is very tight and the device is operated on the edge, as it is likely to happen in practice. This basically includes input pulses of high peak power as well as a large SOA small signal gain, combined with a carrier lifetime that does not leave enough margin for gain recovery in between consecutive data pulses. The representative values of 5 mW, 30 dB and 130 ps used for this purpose result in a large chirp suffering from strong pattern-dependent fluctuations, which are also observed on the amplified pulses, as it is evident in Figs. 5 (left) and 6 (left), respectively. However if the ODI inserts a time delay that falls within the limit specified above then it is possible to reduce the chirp and its peak variations as well as those of the amplified pulses compared to the case of the SOA alone, as it can be seen in Figs. 5 (right) and 6 (right) for $\Delta\tau = 9$ ps. This fact designates the key contribution of the ODI in relaxing the stress governing the SOA dynamic behavior and its negative performance implications on the chirp and the amplified pulses due to the associated pattern effect. On the other hand, the exact extent of chirp suppression is not critical for demonstrating the proof-of-principle of the ODI technique to properly engineer this effect since it depends on the impact that the specific SOA and data characteristics and their combination have on the SOA gain dynamics

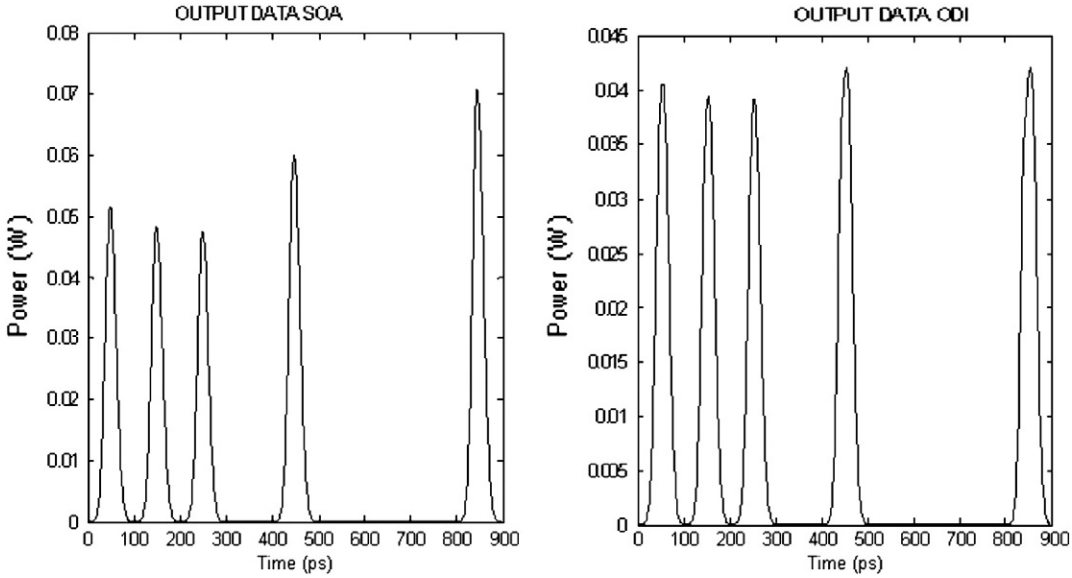

Fig. 6. Amplified output pulse profile for tight SOA working condition in terms of the selected critical parameters, without ODI (left) and with ODI (right) of proper time delay ($\Delta\tau = 9$ ps).

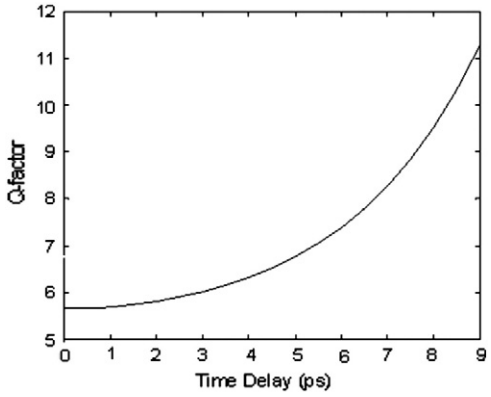

Fig. 7. Q-factor variation versus ODI time delay.

[32,48]. Thus if the amount of chirp becomes larger then the maximum peak chirp variation across the signal coming out from the SOA will be further reduced. Among the possible ways of doing this [32,48], the increase of the SOA linewidth enhancement factor is rather effective as it affects through formula (2) directly the chirp. In fact the change of this parameter from 8 to 12, which is a typical value for SOAs under pulsed operation [49], confirms this improvement, as shown in Fig. 8. Similar results can be obtained by suitably altering the other involved parameters. Additionally, a decrease of the maximum instantaneous frequency deviation of the order observed in Figs. 5 and 8 lies within the dynamic range specified in [48], which gives a measure of the ODI capability to compensate for the chirp. According to [37] such variation is capable of dropping the chirp parameter down to at least the middle of the linear part of its temporal characteristic. Therefore it may be significant for the SOA performance in its considered straightforward amplification applications, especially those like [22]. Finally, it should be mentioned that due to the spectral elimination function of the ODI the inserted PRBS experiences a reduced amplification than without this passive element. This is defined as $(P^{avg}_{out,ODI} - P^{avg}_{in,SOA}) - (P^{avg}_{out,SOA} - P^{avg}_{in,SOA}) = P^{avg}_{out,ODI} - P_{out,SOA}{}^{avg}$ (dB), where $P^{avg}_{out,ODI}$, $P^{avg}_{out,SOA}$ and $P^{avg}_{in,SOA}$ are the PRBS average power calculated at the ODI output and SOA output and input, respectively, taking into account its whole length of 127 bits, and at the optimum specified delay of $\Delta\tau = 9$ ps it is 1.22 dB. This type of penalty is a common characteristic of other techniques also aiming at combating the pattern effect in a SOA employed in its classical role [4,10,11] and constitutes a necessary trade-off that must be made against the efficiency of the filtering action. Nevertheless, it can be practically tolerated by enhancing the signal emerging from the ODI with an optical amplifier operated in the linear gain regime, as in the setups in [11,29], so as to preserve the balance that has been achieved between the peak amplitudes of the data pulses after the ODI. Moreover, the net gain offered by the SOA and ODI combination to the data pulses, $P^{avg}_{out,ODI} - P^{avg}_{in,SOA}$, is under the same working conditions 9.57 dB, which is a level that should be sufficient for transmission or reception purposes. Therefore the overall significant improvements in system performance are not compromised and the ODI can successfully support SOA straightforward amplification.

6. Conclusion

In conclusion the feasibility of employing an ODI to compensate the chirp imposed on RZ pulses amplified by an SOA under conditions of strong pattern effect has been investigated and demonstrated based on a thorough numerical simulation. This has been achieved by describing the SOA behavior by means of a model whose validity and suitability for realistic and accurate predictions has been verified from the succinct comparison with the available experimental evidence. The very good agreement between theory and experiment has allowed to continue with the modeling of the ODI operation using an explicit expression for its phase response whose time derivative defines the chirp. The obtained results and their systematic analysis suggest that placing an ODI in series after the SOA can reduce the magnitude of the chirp and the variations of its peaks together with those of the amplified pulses while ensuring error-free performance enabled by the substantial improvement of the Q-factor. Thus this passive element manages from all perspectives to suppress the pattern effect even when the combination of the critical parameters is challenging for the SOA gain dynamics. However this cannot be done for an arbitrary inserted time delay but for a carefully selected one. This has been found that it should not exceed 1/10th of the repetition period or else the profiles of the amplified pulses are seriously distorted, and the closer this boundary value is approached the better the efficiency of the scheme is. The outcome of this study can be useful for enhancing the performance of applications that exploit the chirp induced by an SOA and simultaneously the SOA potential as straightforward amplification element.

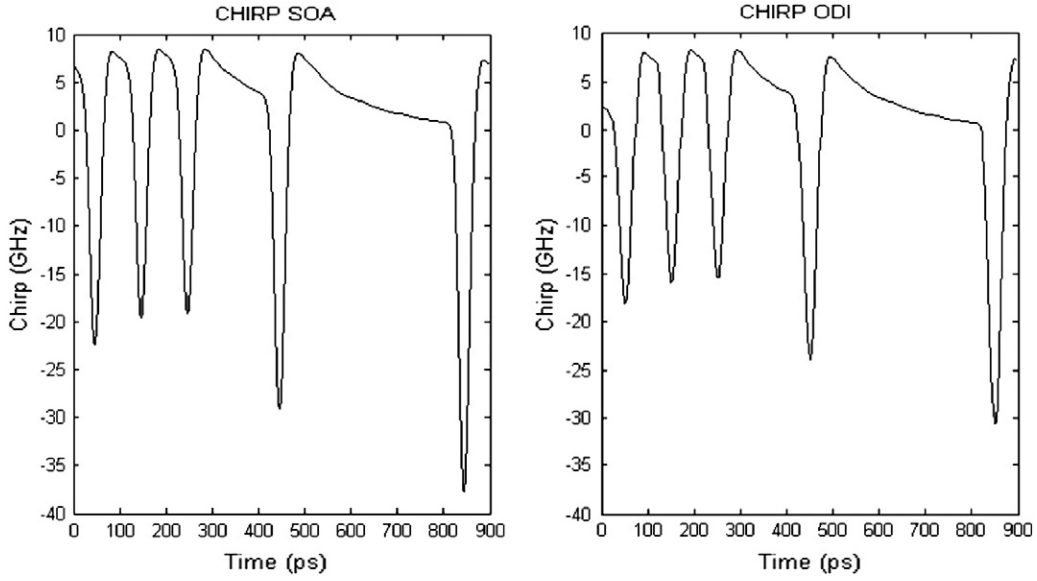

Fig. 8. Amplified output chirp profile as in Fig. 5 but for an increased SOA linewidth enhancement factor.

References

[1] D.R. Zimmerman, L.H. Spiekman, J. Lightwave Technol. 22 (2004) 63.
[2] Y. Kim, H. Jang, Y. Kim, J. Lee, D. Jang, J. Jeong, J. Lightwave Technol. 21 (2003) 476.
[3] X. Wei, Y. Su, X. Liu, J. Leuthold, S. Chandrasekhar, IEEE Photon. Technol. Lett. 16 (2004) 1582.
[4] R. G.-Castrejón, A. Filios, J. Lightwave Technol. 24 (2006) 4912.
[5] M. Kumar, A.K. Sharma, T.S. Kamal, Optik 118 (2007) 34.
[6] S. Singh, R.S. Kaler, Optik 119 (2008) 329.
[7] R. G.-Castrejón, L. Schares, M. Duelk, Opt. Quantum Electron. 40 (2008) 1005.
[8] S. Singh, Opt. Commun. 284 (2011) 828.
[9] J. Mørk, M.L. Nielsen, T.W. Berg, Opt. Photon. News 14 (2003) 42.
[10] K.E. Zoiros, C. O'Riordan, M.J. Connelly, Electron. Lett. 45 (2009) 1187.
[11] K.E. Zoiros, C. O'Riordan, M.J. Connelly, IEEE Photon Technol. Lett. 22 (2010) 221.
[12] K.E. Zoiros, C.L. Janer, M.J. Connelly, Opt. Eng. 49 (2010) (art.no.085005).
[13] K.E. Zoiros, T. Siarkos, C.S. Koukourlis, Opt. Commun. 281 (2008) 3648.
[14] K. Inoue, Electron. Lett. 33 (1997) 885.
[15] J. Yu, P. Jeppesen, J. Lightwave Technol. 19 (2001) 1316.
[16] Q. Xu, M. Yao, Y. Dong, W. Cai, J. Zhang, IEEE Photon. Technol. Lett. 13 (2001) 1325.
[17] K. Chan, C.-K. Chan, W. Hung, F. Tong, L.K. Chen, IEEE Photon. Technol. Lett. 14 (2002) 995.
[18] G.P. Agrawal, N.A. Olsson, IEEE J. Quantum Electron. 25 (1989) 2297.
[19] G.P. Agrawal, Applications of Nonlinear Fiber Optics, Ch. 6, Academic Press, San Diego-CA, 2001.
[20] G.P. Agrawal, N.A. Olsson, Opt. Lett. 14 (1989) 500.
[21] Y. Zhao, P. Ye, Opt. Commun. 199 (2001) 361.
[22] T. Houbavlis, K.E. Zoiros, Optik 114 (2003) 322.
[23] N.Y. Kim, X. Tang, J.C. Cartledge, A.K. Atieh, J. Lightwave Technol. 25 (2007) 3730.
[24] G. Girault, A.M. Clarke, D. Reid, C. Guignard, L. Bramerie, P. Anandarajah, L.P. Barry, J.-C. Simon, J. Harvey, Opt. Commun. 281 (2008) 5731.
[25] E. Tangdiongga, Y. Liu, H. de Waardt, G.D. Khoe, H.J.S. Dorren, IEEE Photon. Technol. Lett. 18 (2006) 908.
[26] J. Dong, X. Zhang, S. Fu, J. Xu, P. Shum, D. Huang, IEEE J. Sel. Top. Quantum Electron. 14 (2008) 770.
[27] J. Dong, X. Zhang, J. Xu, D. Huang, S. Fu, P. Shum, Opt. Exp. 15 (2007) 2907.
[28] J. Dong, S. Fu, X. Zhang, P. Shum, J. Xu, D. Huang, Opt. Commun. 270 (2007) 238.
[29] M.L. Nielsen, J. Mørk, R. Suzuki, J. Sakaguchi, Y. Ueno, Opt. Express 14 (2005) 331.
[30] C.S. Wong, H.K. Tsang, Opt. Commun. 232 (2004) 245.
[31] J. Dong, X. Zhang, F. Wang, W. Hong, D. Huang, Opt. Commun. 281 (2008) 5618.
[32] T. Watanabe, N. Sakaida, H. Yasaka, F. Kano, M. Koga, J. Lightwave Technol. 18 (2000) 1069.
[33] K. Hussain, R. Pradhan, P.K. Datta, Opt. Quantum Electron. 42 (2010) 29.
[34] M.T. Hill, H. de Waardt, G.-D. Khoe, H.J.S. Dorren, IEEE J. Quantum Electron. 39 (2003) 886.
[35] H. Dong, G. Zhu, Q. Wang, H. Sun, N.K. Dutta, J. Jaques, A.B. Piccirilli, IEEE Photon. Technol. Lett. 17 (2005) 303.
[36] D. Derickson, Fiber Optic Test and Measurement, Ch. 5, Prentice Hall Professional Technical Reference, New Jersey, 1997.
[37] K.E. Zoiros, R. Chasioti, C.S. Koukourlis, T. Houbavlis, Optik 118 (2007) 134.
[38] C. Botsiaris, K.E. Zoiros, R. Chasioti, C.S. Koukourlis, Opt. Commun. 278 (2007) 291.
[39] M. Kumar, A.K. Sharma, T.S. Kamal, J.S. Malhotra, Optik 120 (2009) 330.
[40] Z. Li, Y. Dong, C. Lu, Y.J. Wen, Y. Wang, W. Hu, T.H. Cheng, IEEE Photon. Technol. Lett. 18 (2006) 2680.
[41] M. Pauer, P.J. Winzer, W.R. Leeb, J. Lightwave Technol. 19 (2001) 1255.
[42] R. Gutiérrez-Castrejón, M. Dülk, St. Fischer, G. Guekos, Opt. Commun. 192 (2001) 245.
[43] M.G. Kane, I. Glesk, J.P. Sokoloff, P.R. Prucnal, Appl. Opt. 33 (1994) 6833.
[44] J.S. Vardakas, K.E. Zoiros, Opt. Eng. 46 (2007) (art. no. 085005).
[45] Y. Dong, J. Mo, Z. Li, Z. Li, Y. Wang, C. Lu, IEEE Photon. Technol. Lett. 16 (2004) 2359.
[46] S. Singh, R.S. Kaler, Opt. Commun. 266 (2006) 100.
[47] G.P. Agrawal, Fiber-Optic Communication Systems, 3rd ed Wiley, New York, 2002 Ch. 4.
[48] M. Matsuura, N. Iwatsu, K. Kitamura, N. Kishi, IEEE Photon. Technol. Lett. 20 (2008) 2001.
[49] L. Schares, C. Schubert, C. Schmidt, H.G. Weber, L. Occhi, G. Guekos, IEEE J. Quantum Electron. 39 (2003) 1394.